Characterising Group Interaction Modelling for Complex Composite Materials

Nicholas E. Taylor and David M. Williamson

10th June 2019

AWARDING AGENCY: EUROPEAN OFFICE OF AEROSPACE RESEARCH AND DEVELOPMENT
CONTRACT NUMBER: FA9550-17-1-0034

Synopsis

An instrument to measure the heat capacity of isotropic heterogeneous materials has been designed, built and demonstrated. Two distinguishing attributes are the ability to measure as a function of temperature down to 25 kelvin, and the large, circa nine cubic centimetres, sample volumes that are probed.

The former is achieved using liquid helium as a cryogen, and allows for the parameterization and/or validation of polymer models, such as Group Interaction Modelling, down to those temperatures. This is significant because many important physical processes in polymers occur below the boiling point of liquid nitrogen, the most commonly used cryogen, and cannot otherwise be directly observed.

The latter is significant because it permits bulk representative specimens of particulate composites having characteristic length scales of order millimeters to be measured. This is in contrast to the more conventional approach of Differential Scanning Calorimetry which is typically restricted to sample volumes two orders of magnitude smaller.

The accuracy of the instrument has been demonstrated by measuring a wide range of materials of known heat capacity at room temperature, and finding good agreement with the accepted literature. We have measured the heat capacity of the polymer PMMA over the temperature range 25 to 400 K, and the polymer PDMS and PDMS/sugar composites over the temperature range 25 K to 300 K. In all cases we have made comparisons to published data where available, as well as to Group Interaction Modelling predictions of the same.

This instrument operates reliably, and is available for use to gather data on a wide range of materials. It is especially well-suited for the study of isotropic materials heterogeneous on the scale of millimeters, such as particulate composites. In particular it can be used for parametrization of models of thermophysical behaviour, such as Group Interaction Modelling, or else as a severe validation exercise for predictions of the same. Discrepancies point to directions in which the models can be further refined. A number of recommended future avenues of research are presented.

Contents

Introduction

Polymers and granular composites of polymers are important components of weapon systems, as solid fuels, polymer-bonded explosives (PBXs), and structural members. Understanding their mechanical properties at a range of strain rates and temperatures is important to their use.

Group interaction modelling (GIM) gives a physically-based equation of state and constitutive model for polymers. Its physical basis means that a wide range of experiments can provide input to the model. The variation of heat capacity with temperature probes available energy modes, which can be a very information-rich input to GIM.

For most polymers, their lowest transition temperature is in the range 10 K to 100 K. Capturing the polymer's heat capacity around these transitions can help constrain GIM. A helium-cooled system can reach this temperature range relatively simply.

Some composites of interest have characteristic length scales of order a millimetre. This is typically also the maximum size of a sample for use in a differential scanning calorimeter (DSC). A DSC therefore will not probe a representative sample of one of these coarse-grained composites.

A transient plane source (TPS) system measures thermal transport properties: conductivity and diffusivity. These can be combined to give the material heat capacity per unit volume. Unlike a DSC, a TPS sample is of order 10 mm on its shortest dimension.

In this work we use a helium-cooled TPS system to measure heat capacity per unit volume for polymers and polymer composites in the temperature range 30 K to 300 K. This provides information to parameterize a GIM model of those polymers and composites.

In particular, we were interested in the effects on bulk properties of the interface region between a crystal grain and the surrounding polymer binder. Bohn et al. (2019) and Lemos et al. (2017) observed some variation of composite behaviour with filling which could not be fully attributed to a simple rule-of-mixtures composite description of the isolated properties of the matrix and fill.

1 Theory

1.1 Group interaction modelling

Group interaction modelling (GIM) predicts polymer physical properties based on the chemical structure of the monomer unit. The model is de-

scribed in detail in Porter (1995). This section provides a broad overview of the technique, and uses it to develop equations of state for the materials studied in this research.

GIM treats a polymer by considering a 2D hexagonal unit cell consisting of a single monomer unit and its six nearest neighbours in adjacent polymer chains. The polymer chain itself is treated as inextensible: the covalent forces within the chain are one or two orders of magnitude stronger than the van der Waals forces between chains.[1] The potential ϕ between adjacent chains is then taken as a Lennard-Jones 6-12 potential

$$\phi = \phi_0 \left[\left(\frac{r_0}{r} \right)^{12} - 2 \left(\frac{r_0}{r} \right)^{6} \right] \ . \tag{1}$$

The depth ϕ_0 and location r_0 of the potential minimum can be found by summing the contributions of groups in the monomer unit (van Krevelen, 1990). Usually the cohesive energy $E_{\text{coh}} = \phi_0 n_A$ where n_A is Avogadro's number, and the van der Waals volume $V_w = 0.787 r_0^3$, are calculated from standard group-contribution tables. Alternatively, the unit cell used by GIM might prove simple enough to be treated using computational chemistry.

The length L of the monomer unit can be found from molecular modelling, and its molar mass M simply from the unit's chemical formula. The configurational energy due to the inefficient packing of a polymer is treated as a constant multiplier, depending on degree of crystallinity, of E_{coh}.

The thermal energy of the polymer is treated using a simplified Tarasov model (see for example Hartwig (1994); Perepechko (1980)). This requires the Debye temperature for 1D oscillations along the polymer chain, which can be estimated from the tensile modulus of the polymer chain and the molar mass M of a monomer unit.

Most of the time- and temperature-dependence of polymer properties derives from the number of degrees of freedom for atomic motion in the polymer. These are divided into skeletal and atomic modes. Skeletal modes affect the polymer chain and are typically found from the monomer structure. These modes contribute to the Tarasov relation. Atomic modes don't move the centre of mass of the vibrating group, and are therefore treated as independent Einstein oscillators. Atomic modes store heat but make no other contribution to GIM. They are usually identified from infra-red spectroscopy of the polymer.

The activity of degrees of freedom varies with temperature. GIM typically treats this below the glass transition by defining a β transition, with some

[1] A correction for chain compression is necessary at pressures of several gigapascal. It is ignored in this research, all of which takes place at ambient pressure.

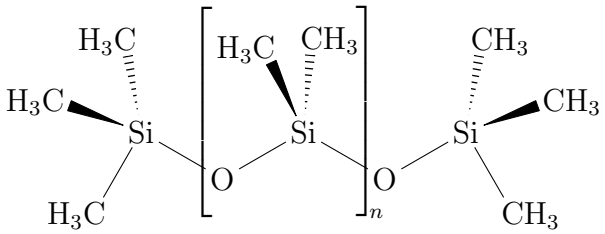

Figure 1: Structure of poly(dimethylsiloxane)

Parameter	**Symbol**	**Value**
van der Waals volume	V_w	$42.6\,\mathrm{cm^3\,mol^{-1}}$
Molar mass	M	74 u/monomer
Unit length	L	3.04 Å/monomer
Cohesive energy	E_{coh}	$15.8\,\mathrm{kJ\,mol^{-1}}$
Debye temperature	θ_1	195 K
Skeletal degrees of freedom	N	8
Chain degrees of freedom	N_c	4
Glass transition width	ΔT_g	6 K
Crystal fraction	f_c	0

Table 1: GIM parameters for PDMS. Note that this model has no beta transition.

width in temperature over which some number of degrees of freedom become available. These transitions are typically significant contributors to polymer toughness.

The glass transition is treated by finding the inflection point of the potential ϕ, at which the potential ceases to pose a barrier to motion of polymer chains past each other. The corresponding conformational, thermal and mechanical energy defines a temperature vs. strain relation above which the polymer is rubbery. In the rubbery state, adjacent molecular chains can move wholesale relative to each other. This increases the number of skeletal degrees of freedom by 50 %.

1.1.1 GIM for PDMS

One of the materials studied in this research was Dowsil Sylgard 184. This is a cross-linked poly(dimethylsiloxane) (PDMS). Figure 1 shows its structure.

Porter (1995) gives parameters for a PDMS model. `GimPDMS` in the attached `gim_tron.py` is a Python implementation of the model. Tables 1 and 2 show the parameters and atomic modes used.

Mode	Number	Temperature / K
$-CH_3$ rock	2	1024
$Si-CH_3$ stretch	2	1024
Asymmetric $Si-O-Si$ stretch	4	1373
Symmetric CH_3 stretch	6	1610
Asymmetric CH_3 stretch	6	3879

Table 2: Atomic modes of PDMS (Efimenko et al., 2002)

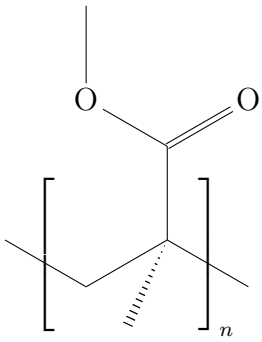

Figure 2: Structure of poly(methyl methacrylate)

1.1.2 GIM for PMMA

Another material studied in this research was poly(methyl methacrylate) (PMMA), a transparent, colourless polymer also known as Plexiglas or Perspex. Figure 2 shows its structure.

Porter and Gould (2009) develops a GIM model for PMMA. This model is implemented in Python as `GimPMMA` in the attached `gim_tron.py`. Tables 3 and 4 show the GIM parameters and atomic modes used in the model.

1.2 Transient plane source

Transient plane source (TPS) is a method of making simultaneous measurements of thermal conductivity and diffusivity, and hence heat capacity per unit volume, in bulk samples. The technique is described in ISO 22007-2:2008, with background detail in Gustafsson (1991).

The technique uses a flat metal-foil resistor to heat the sample and simultaneously to measure the sample temperature. The resistor is embedded in the sample, typically by clamping it between two slabs of the material of interest in a "sandwich" configuration. The thermal resistance of this imperfect contact can be approximated, after a short initial equilibration period,

Parameter	Symbol	Value
van der Waals volume	V_w	$57\,\mathrm{cm^3\,mol^{-1}}$
Molar mass	M	$100\,\mathrm{u/monomer}$
Unit length	L	$3.1\ \text{Å/monomer}$
Cohesive energy	E_{coh}	$45\,\mathrm{kJ\,mol^{-1}}$
Debye temperature	θ_1	$290\,\mathrm{K}$
Beta activation energy	ΔH_β	$70\,\mathrm{kJ\,mol^{-1}}$
Skeletal degrees of freedom	N	6.7
Chain degrees of freedom	N_c	6.7
Beta degrees of freedom	ΔN_β	2
Beta transition width	ΔT_β	$80\,\mathrm{K}$
Glass transition width	ΔT_g	$13\,\mathrm{K}$
Crystal fraction	f_c	0

Table 3: GIM parameters for PMMA

Mode	Number	Temperature / K
C–H stretch	6	4000
C=O stretch	1	2000
C–H scissor bend	8	2000
C–C stretch	2	1500
C–C–H bend	3	1500
O–C–H bend	2	1500
C–H rock	8	1000
C–C–C bend	1	700
C–CH_3 wag	2	700
C–O–C bend	1	500
C–C–C rock	3	500
Ester rotation	1	300

Table 4: Estimated atomic modes in PMMA. From P. J. Gould (personal communication) and Lipschitz (1982).

Figure 3: Hot Disk sensor 5501. Nickel foil (dark regions) encapsulated in kapton. Diameter of double-spiral sensing area is 12.8 mm.

as causing a constant offset ΔT_i between the resistor temperature and that of the sample. If the measurement time is kept sufficiently short, the boundary conditions at the edge of the sample are irrelevant and the sample may be treated as infinite.

For a given resistor geometry and constant heating of the resistor, the heat equation for the system can be solved and rearranged into a form with thermal conductivity K, thermal diffusivity κ, temperature offset ΔT_i and a time offset t_c as fitting parameters. This model can then be fit to the experimental data, yielding K and κ. Heat capacity per unit volume $C_{\text{vol}} = \frac{K}{\kappa}$.

2 Apparatus

Two main pieces of equipment were used in this research: a TPS 3500 thermal constants analyser from Hot Disk AB of Sweden, and a custom-made cryostat.

2.1 TPS 3500

The TPS 3500 comprises all the parts necessary to make transient plane source measurements of thermal properties per ISO 22007-2:2008. It uses interchangeable heater/sensor elements of the form shown in figure 3. The control software uses a database of sensor geometries and a curve-fitting routine to extract thermal constants from the recorded temperature rise.

Sensor radius / mm	Heat capacity / $\mathrm{MJ\,m^{-3}\,K^{-1}}$		
	Steel	Macor	UHMW PE
2.001	3.73 ± 0.16	1.835 ± 0.015	1.516 ± 0.006
6.403	3.78 ± 0.02	1.987 ± 0.010	1.624 ± 0.011
6.403	3.76 ± 0.02	2.050 ± 0.005	1.67 ± 0.03
9.868	—	—	1.65 ± 0.05

Table 5: Heat capacities by sensor radius. Two different sensors of radius 6.403 mm were used. Only UHMW PE was probed using the 9.868 mm sensor. Uncertainties are standard deviations of typically 10–30 measurements.

2.1.1 Effect of sensor

Heater/sensor elements are available in a variety of sizes and substrate materials. For substrate material, we rapidly selected kapton: of the materials available, it was the easiest to work with. Kapton is unsuitable for use above 300 °C, which was not a relevant consideration for this research.

The choice of sensor size was not such a trivial decision. To save space in the cryostat, we wanted the smallest sensor we could use without skewing the results. To assess the effect of sensor size, if any, we used three different sensor designs in three materials with a wide range of heat capacities and thermal conductivities. The sensor designs were Hot Disk numbers 7577, 5501, and 8563, with sensor radii of 2.001 mm, 6.403 mm, and 9.868 mm respectively. The materials used were stainless steel, Macor, and UHMW PE (see section 3). Table 5 shows the results.

These results indicate that, for polymers and ceramics, the 6.403 mm 5501 sensor is appropriate. Radii smaller than this under-reported heat capacity, while larger radii afforded no additional benefit. That sensor was therefore used for all subsequent experiments. The results also suggest that the standard deviation of a set of measurements underestimates the uncertainty in this technique: changing between two nominally identical sensors altered the reported volumetric heat capacity by more than one standard deviation in most cases: 1.7 % versus 2.8 %. Neither are sufficiently large to be a cause for concern.

2.1.2 Effect of force

To assess the effect of clamping force on reported heat capacity, a selection of weights were used to provide well-known clamping forces to various samples.

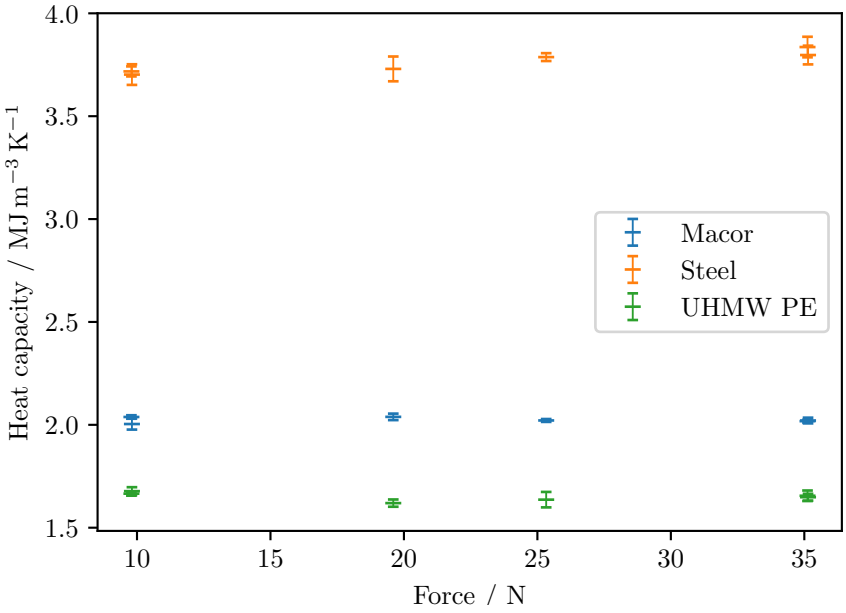

Figure 4: Effect of clamping force on reported volumetric heat capacity.

Figure 4 shows the results. In the range 10 N to 35 N the clamping force has very little effect.

2.1.3 Comparison with literature

Specific heat and density of many materials at room temperature are tabulated in the literature. This allows comparison between the specific heat found with the TPS 3500 and values reported in the literature. Figure 5 shows the comparison. Apart from the very wide variation in literature values of polymer heat capacities, the agreement is very good: perfect agreement would mean that the data points lay exactly on the line $y = x$. As it is, the data points are statistically consistent with such an interpretation. This conclusion is in accord with earlier work on transient plane source systems (Log and Gustafsson, 1995).

2.1.4 Temperature coefficient of resistivity

The heater/sensors used are made from metal foil (Nickel in this instance), and the TPS 3500 control software has a look-up table of resistivity vs. temperature for the sensors in the temperature range −79.5 °C to 750 °C. As this research aims to probe temperatures below that range, it was necessary

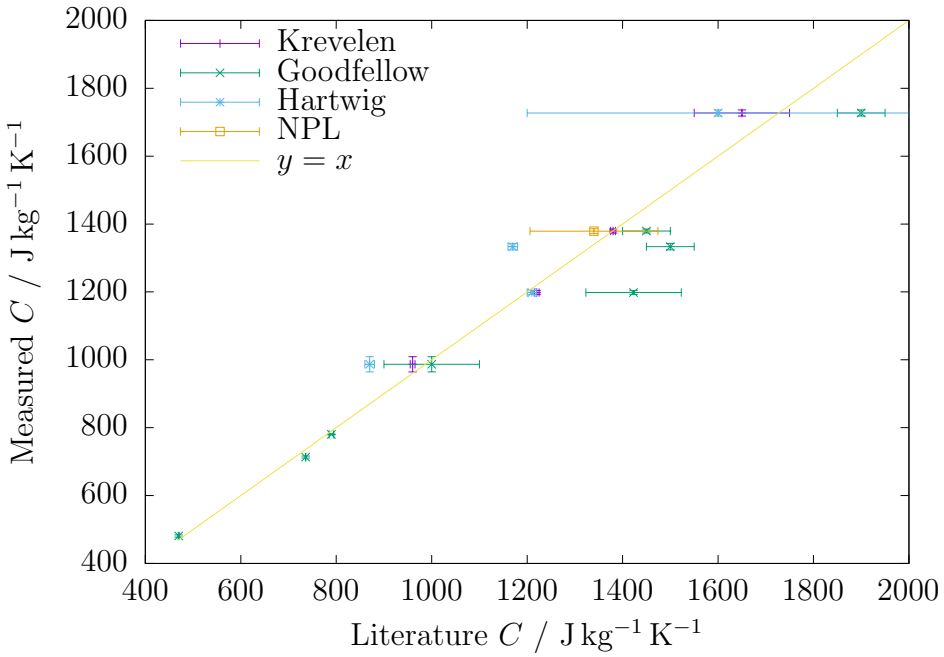

Figure 5: Comparison of literature and measured values of heat capacity. Literature data from van Krevelen (1990); Goodfellow; Hartwig (1994); Rides et al. (2008).

$$
\begin{aligned}
a_0 &= 1.7609 && \Omega \\
a_1 &= -1.3409 \times 10^{-2} && \Omega\,\mathrm{K}^{-1} \\
a_2 &= 4.5844 \times 10^{-4} && \Omega\,\mathrm{K}^{-2} \\
a_3 &= -1.9234 \times 10^{-6} && \Omega\,\mathrm{K}^{-3} \\
a_4 &= 4.6394 \times 10^{-9} && \Omega\,\mathrm{K}^{-4} \\
a_5 &= -4.4004 \times 10^{-12} && \Omega\,\mathrm{K}^{-5}
\end{aligned}
$$

Table 6: Polynomial coefficients for equation (3) for the cryostat 5501 sensor.

for us to extend that calibration to encompass the lowest temperatures used (25 K) by conducting our own calibration experiments.

The sensor to be calibrated was clamped between two copper plates, in which type N thermocouples were embedded. The sensor temperature was taken as the average of the two thermocouple measurements. Temperature was swept across the range of interest, and the sensor resistance measured. The temperature coefficient of resistance is given by

$$\alpha = \frac{1}{R(T_0)} \frac{\mathrm{d}R}{\mathrm{d}T} \ . \tag{2}$$

A polynomial was fitted to the measured $R(T)$, giving a functional form for α of

$$\alpha \approx \frac{\sum_{i=1}^{n} i a_i T^{i-1}}{\sum_{i=0}^{n} a_i T^i} \ . \tag{3}$$

Figure 6 shows the calibration graphically. Note that resistance becomes nearly independent of temperature at 25 K. This characteristic dictates the lowest practical temperature for which meaningful data can be obtained. To measure below 25 K would require a different resistive sensing material, such as Cernox, instead of nickel.

Table 6 shows the polynomial coefficients for equation (3). This was used to tabulate temperature coefficient of resistance across the range of interest at intervals of 1 K, and this table was provided to the TPS 3500 control software as a custom TCR lookup table.

2.2 Cryostat

The choice of 5501 sensor for the TPS 3500 imposed a minimum sample diameter of 25.6 mm: the sample must extend at least one sensor radius in every direction from the sensor. A survey of the major suppliers of commercially-available cryostat systems which permitted this sample size either held the sample in vacuum or were vastly out of the project's budgetary reach. Many

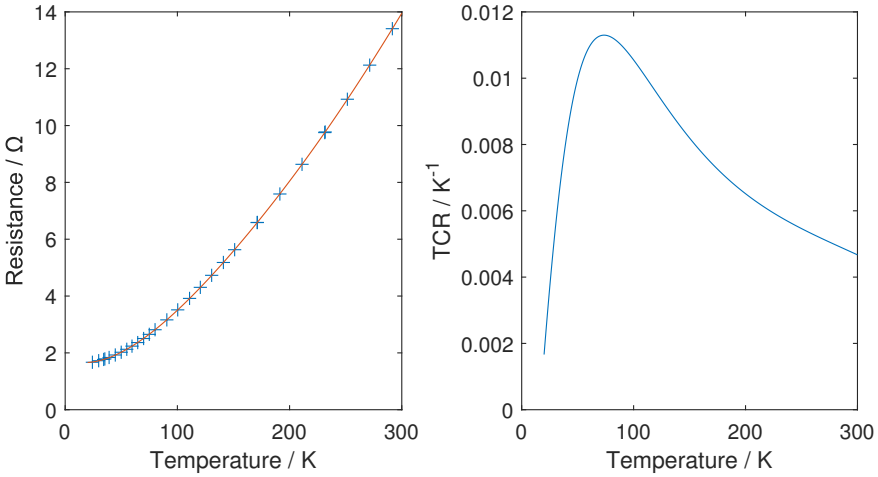

Figure 6: Graphs of resistance (left) and temperature coefficient of resistance (right) vs. temperature for the cryostat 5501 sensor.

potentially interesting materials are soft, porous, and/or have volatile components: properties which make incorporating vacuum an unattractive prospect.

Therefore we constructed a bespoke cryostat of our own design. Rough temperature control was achieved by exploiting the naturally occurring steep vertical temperature gradient arising from gravity-induced stratification in the neck of a liquid helium dewar. It should be noted that the specimen itself experiences a uniform temperature. The sample chamber was moved vertically in the dewar neck manually.

The sample chamber was a 150 mm length of 35 mm copper pipe, with machined end caps. Kapton-insulated resistive heater strips were glued to the outside of this chamber using GE varnish. Fine temperature control was achieved using a Eurotherm 2408 process controller controlling the power supply to these heater strips. Figure 7 shows the system schematically, and the attached `Cryo-breakdown.mp4` video shows a breakdown of the system.

The end result provided a cylindrical specimen compartment, 131 mm long and 32.7 mm in diameter. Six type N thermocouples were used to assess the temperature distribution in this volume, and found that the bottom 70 mm had a uniform temperature to within 1 K.

The limited diameter of the specimen compartment required that the sample be mounted vertically. Clamping the sample presented a problem: differential thermal expansion between the sample and a rigid clamp would leave the sample completely loose at low temperature. The easiest solution,

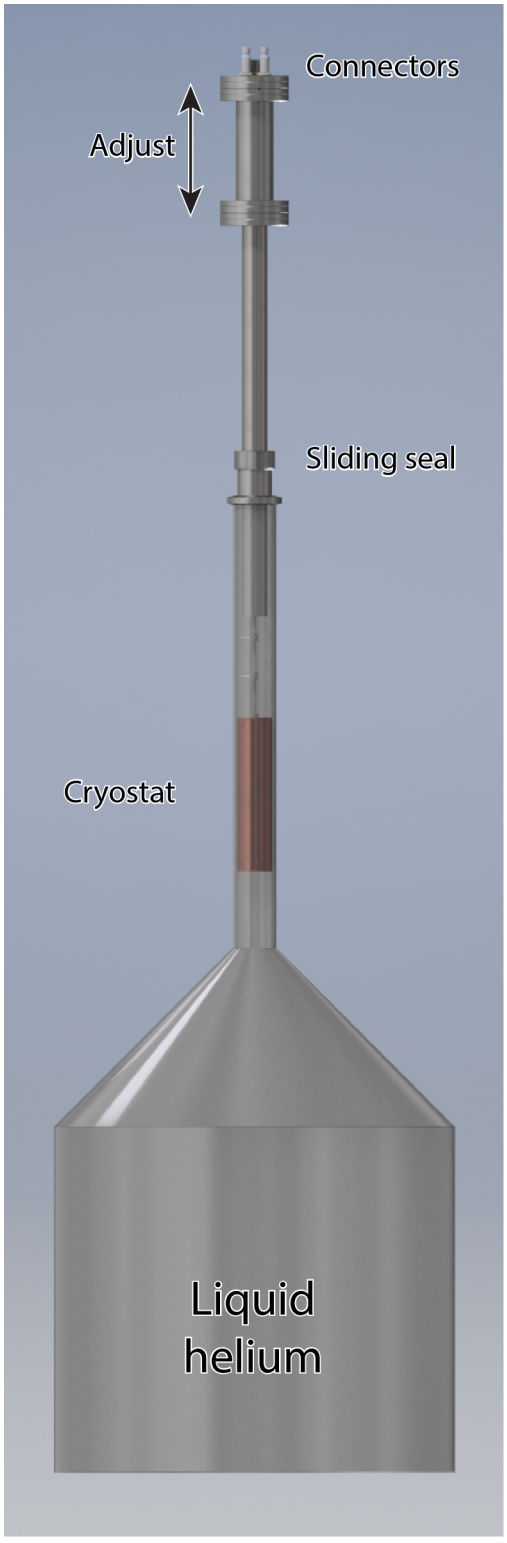

Figure 7: Schematic of cryostat

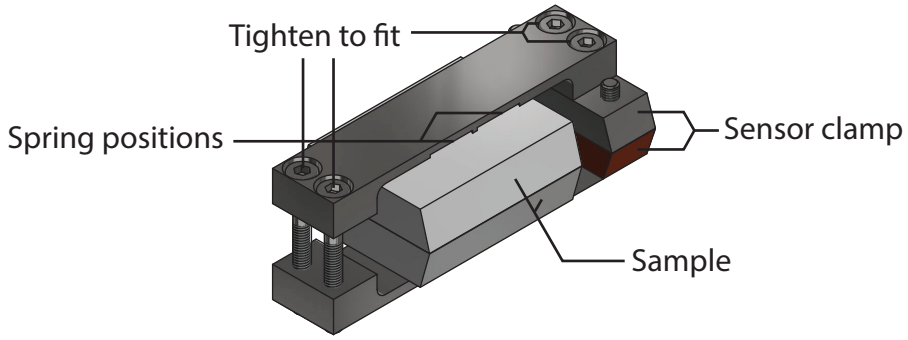

Figure 8: Sample clamping system for use in cryostat. Total length 65 mm. In the cryostat, down is left and out of the page.

of putting a weight on top of the sample, was precluded by the vertical mounting. Instead, the sample was mounted using three stainless steel conical springs on each side providing 30 N to 90 N of clamping force. Changes in the sample dimensions will have relatively little effect on the clamping force, and the elastic modulus of stainless steel changes only slightly between room temperature and 4.2 K (Ledbetter et al., 1975). The results in section 2.1.2 provide confidence in the suitability of this approach. Figure 8 illustrates the system.

3 Samples

Several materials were probed in this research. Most were only studied at room temperature to establish confidence in the apparatus, populating figure 5. The materials and their provenances were:

- Stainless steel, SIS 2343, supplied with TPS 3500 instrument for validation.
- Fused silica, Thorlabs mirror blank PF20-03.
- Macor machinable ceramic, Dow Corning.
- Cross-linked polystyrene, Goodfellow Cambridge Ltd. ST303150/5
- Polytetrafluoroethene (PTFE), Goodfellow Cambridge Ltd. FP303220/1
- Polymethylmethacrylate (PMMA), Goodfellow Cambridge Ltd. ME303120/1

- Polyoxymethylene (POM), Goodfellow Cambridge Ltd. OX313100/1
- Ultra-high molecular weight polyethylene (UHMW PE), Goodfellow Cambridge Ltd. ET303200/1
- Polydimethylsiloxane (PDMS), Dow Corning Sylgard 184. 10:1 mix, 48 hour room temperature cure.
- Food-grade sugar crystals, ∼10 mm diameter. This was never probed in isolation, but only used to manufacture PDMS/sugar composite samples.

For experiments at room temperature and above, samples were typically of order 50 mm across and 12 mm to 25 mm thick. This was significantly larger than the region probed by the TPS 3500, fulfilling the boundary-condition requirements that the sample extent appear infinite to the probe. For experiments in the cryostat, samples were trapezium-section prisms, 35 mm deep, 30 mm wide on their long face, 25.7 mm wide on their shorter face, and 7.7 mm thick. A pair of these, of identical material, were clamped together around the transient plane source heater/sensor. This shape was chosen to maximize the available probing depth (minimum distance between the sensor and a sample edge), without requiring any curved surfaces to be machined. It was not practical to machine PDMS and PDMS/sugar composites; instead they were moulded as a cuboid containing this shape, and the angled faces cut with a scalpel. These trapezoid specimens also met the boundary condition requirements of the TPS 3500.

The materials probed away from ambient temperature were PMMA, PDMS and a variety of PDMS/sugar composites. Manufacture of PMMA and PDMS specimens was straightforward and repeatable.

3.1 PDMS/sugar composites

We chose PDMS and sugar as the components of our granular composite system because they are readily available, relatively easy to work with, and of very low toxicity. The intention was to vary the specific interface area in our composite without changing its composition, keeping the volume fractions constant. The simplest way to do this was by varying the crystal size; if the crystal shape and volume fraction remains constant and crystal-on-crystal contact is neglected, specific interface area is inversely proportional to crystal diameter.

The first problem we encountered when making PDMS/sugar composites was that most powdered sugar contains anti-caking agents. Since these

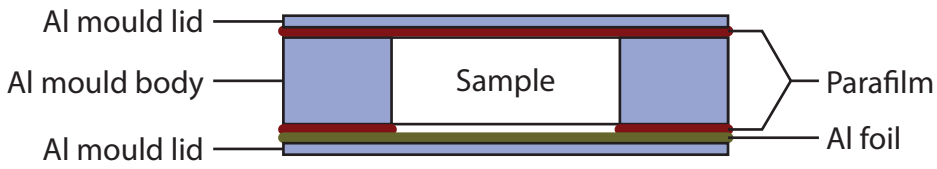

Figure 9: Section of mould for PDMS/sugar composites, showing parafilm seals and aluminium foil release layer. Lids are held in place with bolts (not shown).

modify the surface properties of the sugar and it is precisely those properties in which we were interested, this presented a problem. We therefore chose to use sugar crystals very much larger than the grain size we planned to study, reasoning that any surface treatment would then be a small component of our material and independent of crystal size. These large crystals were ground using a pestle and mortar. Size fractions were extracted using stainless steel laboratory sieves and an automated shaker.

We selected two size fractions:

- "Fine" sugar that passed a 63 µm sieve and was retained on a 45 µm sieve.
- "Coarse" sugar that passed an 800 µm sieve and was retained on a 500 µm sieve.

Samples were cast in an aluminium mould with removable top and bottom faces. The mould cavity was 7.8 mm deep, in the shape of a 35 by 60 mm rectangle with rounded corners of radius 5 mm. The bottom face was sealed against the mould body with a layered system of aluminium foil and "Parafilm M" laboratory wrapping film shown in figure 9. The sample region was then filled with the desired amount of sieved sugar, liquid PDMS precursor added, and the mixture de-gassed (see section 3.1.2). The sample cell was then sealed using more parafilm, taking care not to trap bubbles, and the top face bolted down.

3.1.1 Sedimentation

In an attempt to prevent sedimentation during the 48 h curing time of the PDMS, the sealed cell was rotated in a modified "Turbula" powder mixer from Willy A. Bachofen AG of Switzerland. The modifications reduced the mixer's speed to about one revolution per thousand seconds. This prevented

sedimentation of fine sugar at 5.8 % fill fraction (8.7 % by weight), and of coarse sugar at 40 % fill fraction (50 % by weight).

Coarse sugar at 5.8 % fill fraction, however, reliably sedimented, generating a roughly linear density gradient across the sample. Speeding up the powder mixer to 35 s and then to 6 s per revolution resulted in less even distribution of coarse sugar. Reducing the mould cavity to a 27 mm diameter circle also failed to eliminate sedimentation. It did, however, reduce it significantly and some measurements were taken with this smaller sample size.

3.1.2 Degassing

Powder beds tend to entrain air, and Sylgard 184 precursor is a very viscous liquid. To eliminate the effect of different air entrainment between coarse and fine beds, we degassed the samples in vacuum. Initially we took advantage of Sylgard 184's two-component nature, mixing the resin with sugar and degassing with no time pressure, before adding the curing agent and mixing that in. However it proved difficult to mix the curing agent with the sugar-filled resin without entraining additional air. This resulted in several unevenly-cured samples.

We therefore instead pre-mixed the resin and curing agent, degassed the mixture, and added the mixed Sylgard 184 to the sugar, before degassing the sugar/Sylgard mix.

4 Methods

Samples were loaded into the cryostat. To keep the springs of the cryostat clamp from digging into the samples, a 1 mm thick by 25 mm square aluminium plate was placed against each side of the sample package. This will not affect the results: the sample surface is outside the probed region of the TPS 3500. A type N thermocouple was affixed to each of these plates, and the average of the two thermocouple readings was taken as the sample temperature. Another type N thermocouple was held in free space near the sample package, and used as the temperature feedback for the Eurotherm process controller. Three more type N thermocouples were spread vertically through the cryostat tube to confirm temperature uniformity in the sample chamber.

The cryostat temperature was then varied between 25 K and 290 K, and measurements of the sample's volumetric heat capacity taken. PMMA was also probed above ambient temperature, using a fan-assisted laboratory oven.

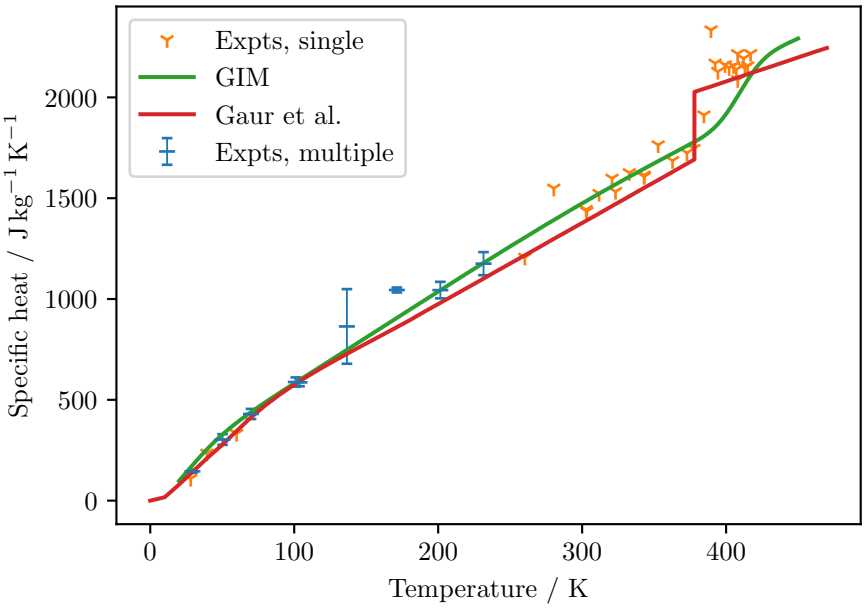

Figure 10: PMMA results compared against GIM and recommended values from Gaur et al. (1982). Note the signature of the glass transition near 400 K. Error bars in "Expts, multiple" are the standard deviation of multiple experiments at a single temperature.

5 Results

5.1 PMMA

The results for PMMA are shown in figure 10. The GIM prediction for PMMA density was used to convert our measured volumetric heat capacity (MJ m^{-3} K^{-1}) into specific heat (J kg^{-1} K^{-1}). We have reasonable agreement with GIM, except near the glass transition temperature. We observe the glass transition to occur over the temperature range 376 K to 389 K, in accord with the figure of 380 K of Gaur et al. This is slightly below the 410 K predicted by GIM. In the range 200 K to 300 K both our results and GIM give heat capacities slightly higher than those reported by Gaur et al.

5.2 PDMS

The results for PDMS are shown in figure 11. GIM predictions of density were again used to convert our measurements to a specific heat. We observe the glass transition to occur over the temperature range 140 K to 150 K, in

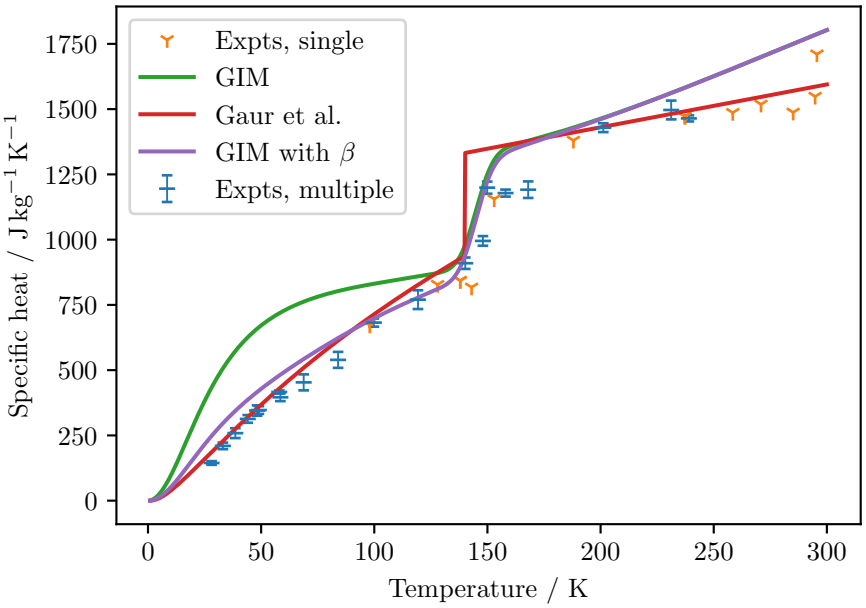

Figure 11: PDMS results compared against textbook GIM, modified GIM (see body text), and recommended values from Gaur et al. (1983). Note the signature of the glass transition near 150 K. Error bars in "Expts, multiple" are the standard deviation of multiple experiments at a single temperature.

good agreement with Gaur et al. (140 K) and GIM (136 K to 153 K). Apart from identically at the glass transition where there is good agreement, the textbook GIM model otherwise significantly over-predicts the experimentally observed values.

The disagreement between GIM and experiment below the glass transition can be improved by adding a beta transition, with activation energy 20 kJ mol^{-1}, freezing four degrees of freedom, and with a width of 50 K. This is physically plausible, and we have been unable to find data in the literature covering transitions of PDMS below 100 K to either support or refute such a supposition: dynamic mechanical analysis (DMA) measurement of the loss tangent in that temperature range would be the easiest way to falsify our prediction.

A GIM model for PDMS with this extra transition is implemented as `GimPDMSBeta` in the attached `gim_tron.py` file.

We have no ready explanation for the discrepancy between GIM and experiment above the glass transition.

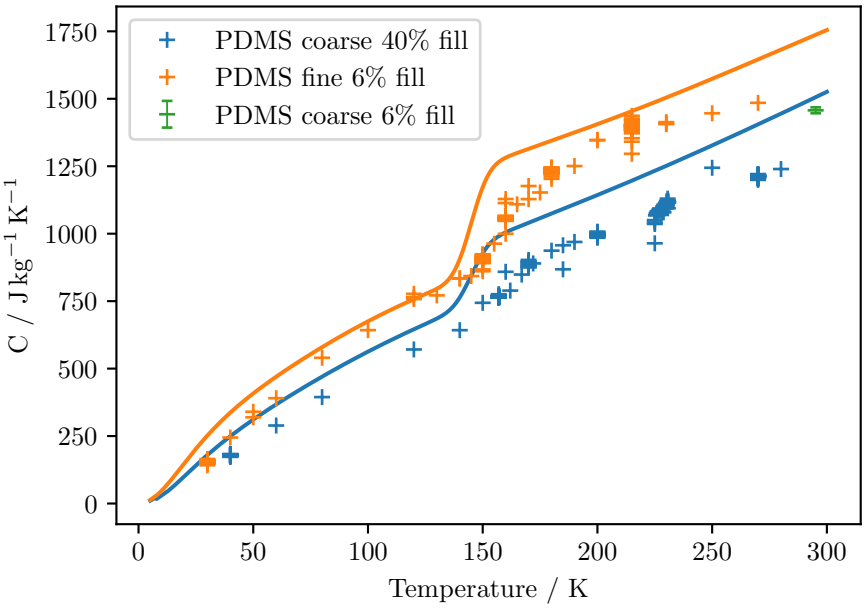

Figure 12: PDMS sugar results. Points are experimental, lines are a model (see body text) for points of the same colour.

5.3 PDMS/sugar composites

The results for PDMS/sugar composites are shown in figure 12. To find the density and convert our measured volumetric heat capacities into specific heats, the PDMS was modelled using the GIM model with beta transition developed above. The sugar was taken to remain at its ambient-temperature density of 1590 kg m^{-3}: as a crystal, its coefficient of thermal expansion should be at least an order of magnitude smaller than that of PDMS.

Putnam and Boerio-Goates (1993) measured the specific heat of sugar from 5 K to 342 K. A model using their experimental values for the sugar and GIM for the PDMS is also shown in figure 12. The model is somewhat unsatisfactory, overestimating the material's heat capacity by order 10 % at all temperatures. However, it does have the virtue of having the correct, albeit stretched on the y-axis, functional form. A Python implementation is provided as `GimPDMSSugar` in the attached `gim_tron.py` file.

Efforts to produce a completely even dispersion of 6 % coarse sugar in PDMS were unsuccessful. Notwithstanding, the most evenly dispersed sample pair was probed at room temperature. Interestingly its heat capacity appears to be slightly below that of fine sugar in PDMS at the same fill fraction. This may be an artefact of the density gradient resulting from uneven dispersion

of the sugar crystals, or it may be evidence of an effect of specific interface on heat capacity.

Cryostat experiments on this coarse PDMS/sugar sample could not be justified in terms of time and consumable expense. We are refraining from incurring this expenditure until such time as we can fabricate more satisfactory samples. This is a promising area to re-visit.

6 Conclusions

The TPS 3500 and cryostat are an effective combination for probing isotropic composites heterogeneous on the millimetre scale, an attribute that distinguishes it from conventional differential scanning calorimetry. This provides usable input to polymer models, in particular group interaction modelling (GIM). It also serves as a severe validation exercise for predictions of the same, as demonstrated in this report. Discrepancies point to directions in which the models can be further refined.

PDMS/sugar mixes have lower heat capacities than the sum of their components, based on existing experimental data on sugar and a rudimentary GIM model.

There is weak evidence that reducing interfacial area in PDMS/sugar mixes while keeping composition constant reduces the heat capacity of the mixture.

7 Future work

The apparatus works reliably and is available for use to gather data on a wider range of materials. It is especially well-suited for the study of isotropic materials heterogeneous on the scale of millimetres, such as particulate composites.

Presently, the instrument provides for measurements of volumetric heat capacity. Highly complementary to this would be a direct measurement of thermal expansion over the same temperature range. Trivially, this would allow for calculation of specific heat without recourse to a material model of density. More importantly, it could wholly constrain any such model, allowing for a fully experimental parameterization.

Separately, we are presently unable to say with confidence whether specific interface area affects measured heat capacity. This is because our samples displayed slight sedimentation. We would like to remedy this and revisit this area of investigation.

Acknowledgements

We are grateful to Cheng Liu of the quantum matter group at the Cavendish Laboratory, and Peter Gould of QinetiQ, for several helpful discussions about cryostat design and group interaction modelling, respectively.

References

Manfred A. Bohn, Mauricio Ferrapontoff Lemos, and Guenter Mussbach. Characterizing of glass-rubber transition shift in filled HTPB-IPDI formulations by modified and normal Arrhenius equation. In *New Trends in Research of Energetic Materials*, pages 52–61, Czech Republic, 2019.

Kirill Efimenko, William E. Wallace, and Jan Genzer. Surface modification of Sylgard-184 poly(dimethyl siloxane) networks by ultraviolet and ultraviolet/ozone treatment. *Journal of Colloid and Interface Science*, 254: 306–315, 2002. doi:10.1006/jcis.2002.8594.

Umesh Gaur, Suk-fai Lau, Brent B. Wunderlich, and Bernhard Wunderlich. Heat capacity and other thermodynamic properties of linear macromolecules. VI. Acrylic polymers. *Journal of Physical and Chemical Reference Data*, 11(4):1065–1089, 1982.

Umesh Gaur, Suk-fai Lau, and Bernhard Wunderlich. Heat capacity and other thermodynamic properties of linear macromolecules. IX. Final group of aromatic and inorganic polymers. *Journal of Physical and Chemical Reference Data*, 12:91–108, 1983.

Goodfellow. Data sheets.

S. E. Gustafsson. Transient plane source techniques for thermal conductivity and thermal diffusivity measurements of solid materials. *Review of Scientific Instruments*, 62(3):797, 1991.

Günther Hartwig. *Polymer Properties at Room and Cryogenic Temperatures*. The International Cryogenics Monograph Series. Plenum, New York, 1994.

ISO 22007-2:2008. *Plastics – Determination of thermal conductivity and thermal diffusivity – Part 2: Transient plane heat source (hot disc) method*. International Organization for Standardization, Geneva, CH, 2008.

H. M. Ledbetter, W. F. Weston, and E. R. Naimon. Low-temperature elastic properties of four austenitic stainless steels. *Journal of Applied Physics*, 46:3855, 1975.

Mauricio Ferrapontoff Lemos, Günter Mussbach, and Manfred August Bohn. Evaluation of filler effects on the dynamic mechanical behavior of HTPB-elastomer used as binder in exemplary composite formulations. *Journal of Aerospace Technology and Management*, 9(3):379–388, 2017.

Irving Lipschitz. The vibrational spectrum of poly(methyl methacrylate): a review. *Polymer-Plastics Technology and Engineering*, 19(1):53–106, 1982. doi:10.1080/03602558208067727.

T. Log and S. E. Gustafsson. Transient plane source (TPS) technique for measuring thermal transport properties of building materials. *Fire and Materials*, 19:43–49, 1995.

I. I. Perepechko. *Low Temperature Properties of Polymers*. Mir Publishers, Moscow, 1980.

David Porter. *Group Interaction Modelling of Polymer Properties*. Marcel Dekker, 1995.

David Porter and Peter J. Gould. Predictive nonlinear constitutive relations in polymers through loss history. *International Journal of Solids and Structures*, 46:1981–1993, 2009.

Robert L. Putnam and Juliana Boerio-Goates. Heat-capacity measurements and thermodynamic functions of crystalline sucrose at temperatures from 5 K to 342 K. revised values for $\Delta_f G^\circ_m$(sucrose, cr, 298.15 K), $\Delta_f G^\circ_m$(sucrose, aq, 298.15 K), S°_m(sucrose, aq, 298.15 K); and $\Delta_r G^\circ_m$(298.15 K) for the hydrolysis of aqueous sucrose. *Journal of Chemical Thermodynamics*, 25:607–613, 1993.

M. Rides, J. Morikawa, L. Hälldahl, B. Hay, H. Lobo, and A. Dawson. Intercomparison of thermal conductivity and thermal diffusivity measurements of polymers. In *Proceedings of the Polymer Processing Society 24th Annual Meeting – PPS-24*, pages S17–958, June 2008.

D. W. van Krevelen. *Properties of Polymers*. Elsevier, third edition, 1990.